Journal of Solid State Electrochemistry (2022) 26:1961–1968
https://doi.org/10.1007/s10008-022-05225-8

ORIGINAL PAPER

High critical currents for dendrite penetration and voiding in potassium metal anode solid-state batteries

Dominic Spencer Jolly[1] · Johann Perera[1] · Shengda D. Pu[1] · Dominic L. R. Melvin[1,2] · Paul Adamson[1,2] · Peter G. Bruce[1,2,3,4]

Received: 1 June 2022 / Revised: 9 June 2022 / Accepted: 11 June 2022 / Published online: 30 June 2022

Abstract
Potassium metal anode solid-state cells with a K-beta"-alumina ceramic electrolyte are found to have relatively high critical currents for dendrite penetration on charge of approximately 4.8 mA/cm^2, and voiding on discharge of approximately 2.0 mA/cm^2, at 20 °C under 2.5 MPa stack-pressure. These values are higher than generally reported in the literature under comparable conditions for Li and Na metal anode solid-state batteries. The higher values for potassium are attributed to its lower yield strength and its readiness to creep under relatively low stack-pressures. The high critical currents of potassium anode solid-state batteries help to confirm the importance of the metal anode mechanical properties in the mechanisms of dendrite penetration and voiding.

Introduction

Solid-state batteries (SSBs) combining a lithium metal anode with a ceramic solid electrolyte (SE) promise to deliver a step change in the energy density of batteries [1, 2]. However, dendrite penetration into the ceramic electrolyte and void formation at the Li/SE interface at moderate (practical) rates of charge and discharge, respectively, limit SSB performance [3–12]. Previous studies have identified that there are two critical currents for metal anode/SE interfaces; a critical current for plating the metal anode at which dendrites will penetrate into the SE, and a critical current for stripping at which voids will nucleate and grow in the lithium metal at the anode/SE interface [13]. Whilst the critical current for dendrite growth has previously received a great deal of attention as it limits the fast-charge capability of SSBs, the formation of voids when stripping the metal anode during discharge is at least as important, perhaps more so, as the critical current for voiding is often lower, and can also lead to cell failure. When the critical current for voiding is exceeded, contact loss between the metal anode and SE will worsen as the battery is cycled, resulting in high local current densities which will give rise to dendrite growth on charging [13].

A number of mechanisms have been proposed to explain how dendrites and voids form at the metal anode/SE interface, and these emphasise the importance of the mechanical properties of the metal anode in determining critical currents. Lower yield strength metals that creep more readily are expected to enable higher critical currents for both dendrite penetration and voiding, as the metal creep rate to the interface during stripping will be higher for the same pressure and temperature, whilst the ability of the softer metal to crack the ceramic on plating is less [14–17]. The observation that Na metal anode SSBs have in general higher critical currents than Li metal anode SSBs supports this, with recent reports that the critical current for dendrite growth is 3–12 mA/cm^2 for the Na/Na-beta"-alumina interface and that the critical current for voiding can be 1.5 mA/cm^2 under 4 MPa stack pressure and 2.5 mA/cm^2 under > 9 MPa [16, 18]. An alternative approach to achieving high critical currents has been to raise the temperature of the cell, as Li metal yields and creeps

For the special issue dedicated to the 70th birthday of Doron Aurbach.

Dominic Spencer Jolly and Johann Perera contributed equally to this work.

✉ Peter G. Bruce
peter.bruce@materials.ox.ac.uk

[1] Department of Materials, University of Oxford, Oxford OX1 3PH, UK

[2] The Faraday Institution, Didcot OX11 0RA, UK

[3] The Henry Royce Institute, University of Oxford, Oxford OX1 3RQ, UK

[4] Department of Chemistry, University of Oxford, Oxford OX1 3TA, UK

more readily at higher temperatures. Moderately elevated temperatures have been found to increase the critical currents for both dendrite growth and void formation [17], and semi-solid alkali metal electrodes such as Li-Na–K have been shown to increase the critical current for Li dendrite growth to 3.5 mA/cm^2 [14]. Taken to the extreme, operating cells at high temperatures with molten metal anodes can enable current densities in the order of A/cm^2 [15].

In this context, it is interesting to study K metal anode SSBs, as K metal has a lower yield strength and creeps more readily than Li and Na metal [14]. We reveal that K anode SSBs utilising a K-beta"-alumina solid electrolyte can achieve a critical current for dendrite growth of approximately 4.8 mA/cm^2, and a critical current for voiding of approximately 2.0 mA/cm^2, under 2.5 MPa stack-pressure at 20 °C, with these results providing further evidence for the importance of the metal anode mechanical properties in the failure of SSBs. In addition, an optimised surface preparation of K-beta"-alumina is described, with surface grinding followed by heat-treatment at 875 °C in an argon atmosphere shown to minimise the interfacial resistance between the K-beta"-alumina and K metal anode by removal of carbonate impurities from the surface of the ceramic.

Experimental

K-beta"-alumina disks was chosen as the SE for this study as it both highly ionically conductive (~ 1 mS/cm) and stable against a K anode meaning that it is possible to assign changes in cell voltage to mechanical changes at the interface (dendrites and voids), rather than electrochemical degradation [14, 19, 20]. K-beta"-alumina disks (Ionotec) were prepared by grinding with successively finer grades of SiC paper. Disks that were to undergo heat-treatment were transferred into an argon-filled glovebox where they were heated in a box furnace (MTI) to the target temperature at a rate of 4 °C/min, held for 4 h and then cooled at 4 °C/min. K-beta"-alumina disks were constructed into 2-electrode cells by affixing 5 mm diameter K foils to each side of the disks, and 3-electrode cells were made by further addition of a 1-mm-diameter K reference electrode. Electrode areas were kept constant by using polypropylene masks to control the K/K-beta"-alumina contact area. Pouch cells with stainless-steel current collectors were vacuum-sealed and removed from the glovebox for testing. Stack-pressure was applied to the cells using sprung clamps, with the pressure set using a piezoelectric pressure sensor (OMEGA).

Electrochemical testing was carried out using a Gamry 1010E potentiostat. Potentiostatic electrochemical impedance spectroscopy (PEIS) was carried out in a frequency range of 1 MHz–1 Hz taking 10 points per decade, using a 10 mV perturbation. Impedance analysis was carried out using the ZView software package. Cell cycling was conducted at 20 °C under a 2.5 MPa stack-pressure. 3-Electrode cycling began by plating the working electrode (and stripping the counter electrode).

Samples were prepared for scanning electron microscopy (SEM) in an argon-filled glovebox and transferred to the SEM (Zeiss Merlin) using an air-tight transfer device (Gatan). Energy dispersive X-ray spectroscopy (EDS) was carried out with a probe current of 200 pA and acceleration voltage of 10 kV using an Oxford Instruments detector and was analysed using the Aztec software package.

Results and discussion

Surface preparation of K-beta"-alumina

Alkali oxide ceramic electrolytes invariably have impurities present on their surfaces, such as carbonates and hydroxides [18, 21, 22]. These impurities are poor ionic conductors and so it is important to remove them when preparing the SE, to minimise the impedance to K-ion transport across the K/K-beta"-alumina interface and to maximise the critical currents.

A combination of grinding and heat-treatment is the most common surface preparation method for Li-ion and Na-ion conducting oxide ceramic electrolytes, and so this method was used to prepare the surface of K-beta"-alumina [16, 18, 21]. K-beta"-alumina disks were ground as described in the Experimental section, before being heat-treated in an argon atmosphere at a range of temperatures between 200 and 950 °C. To assess the results of these heat-treatments, the K-beta"-alumina disks were incorporated into symmetric K/K-beta"-alumina/K cells, and potentiostatic electrochemical impedance spectroscopy (PEIS) was carried out to determine the impedance of the cells (Fig. 1a). The total impedance was observed to decrease from the K-beta"-alumina that was treated at the lowest temperature of 200 °C (red) to a minimum for the K-beta"-alumina disk heat-treated at 875 °C (purple), before showing a slight increase again to the disk heat-treated at 950 °C (grey). A more detailed analysis was carried out by modelling each Nyquist plot to an equivalent circuit model consisting of two resistors in series, each in parallel with a constant phase element, as has been used to interpret impedance spectra for other metal anode/oxide solid electrolyte interfaces (Fig. 1b) [18, 21, 23]. Each resistor in parallel with a constant phase element was used to model a physical processes within the cell which was assigned according to its characteristic capacitance [24]. These were, from high to low frequency, the impedances of the K-beta"-alumina electrolyte and the K/K-beta"-alumina interface. From the fitting of the equivalent circuit to the impedance, it is clear that the decrease in cell impedance

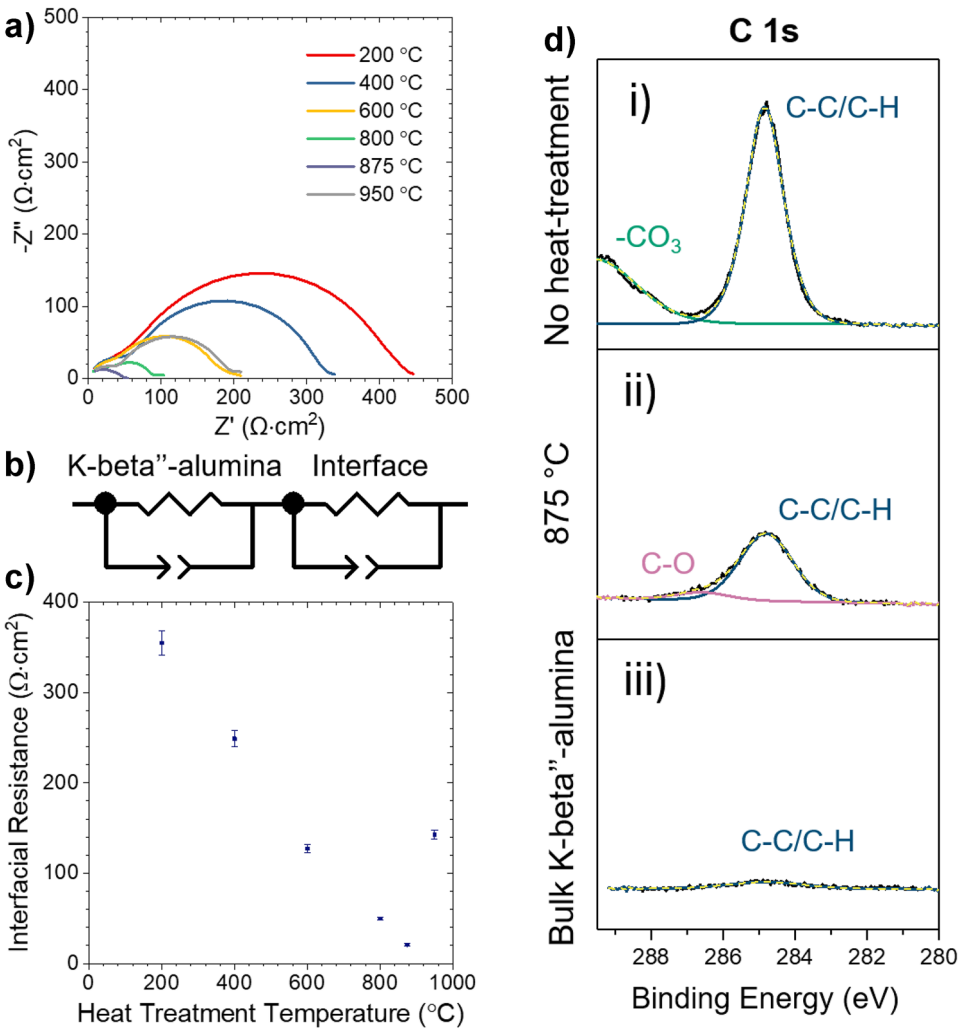

Fig. 1 **a** Nyquist plot showing the impedance of K/K-beta"-alumina/K cells after heat-treatment of K-beta"-alumina at different temperatures. **b** Equivalent circuit model, showing two resistors each in parallel with a constant phase element, which was used to model K/K-beta"-alumina/K impedance spectra. **c** Plot showing the modelled K/K-beta"-alumina interfacial resistances. **d** C 1 s region of the X-ray photoelectron spectra of K-beta"-alumina (i) after no heat-treatment; (ii) after heat-treatment at 875 °C; and (iii) of bulk K-beta"-alumina, showing raw data (black), the total fitting (dashed yellow) and fittings of $–CO_3$ (green), C–C/C-H (blue) and C-O (pink)

with increasing heat-treatment temperature is a result of a decrease in K/K-beta"-alumina interfacial resistance from a maximum of approximately 355 Ω·cm^2 after heat-treatment at 200 °C, to a minimum of 21 Ω·cm^2 when heat-treated at 875 °C (Fig. 1c).

X-ray photoelectron spectroscopy (XPS) was used to relate the decrease in interfacial resistance with heat-treatment to the impurities present on the surface of the K-beta"-alumina. XPS was carried out as described in the Experimental section, and these data are shown in Fig. 1d, which compares the key C 1 s region of the spectra for an untreated K-beta"-alumina surface (Fig. 1di), the surface of a K-beta"-alumina disk that had been heat-treated at 875 °C (Fig. 1dii) and the bulk of K-beta"-alumina which was accessed by sputtering off the K-beta"-alumina surface within the XPS chamber (Fig. 1diii). For the surface of the untreated K-beta"-alumina disk, fitting of the XPS spectrum shows the presence of carbonates (green, 289.5 eV) [25]. However, after heat-treatment at 875 °C, no carbonate remains present on the surface, although a very small concentration of an impurity containing a C-O bond is present (pink, 286.6 eV) [26]. Taken together with the results of the PEIS analysis, it is clear that just as in the cases of the Li/LLZO and Na/Na-beta"-alumina interfaces, decreasing interfacial resistance with heat-treatment is a result of a decrease in concentration of carbonate impurities on the surface of the oxide ceramic [16, 18, 21]. Interestingly, the K/K-beta"-alumina interfacial resistance was observed to increase again when heat-treatment was carried out at 950 °C (Fig. 1c), perhaps due to surface reactivity with minor atmospheric impurities at this high temperature. XPS data for the corresponding O 1 s, Al 2p and K 2p regions of the spectra are shown in Supplementary Fig. 1 for reference.

Critical currents for plating and stripping

Having optimised the surface treatment of K-beta"-alumina, cells were tested to determine the critical current densities of plating and stripping K metal at the K/K-beta"-alumina interface. Firstly, the critical current for dendrite growth was determined using a well-established method; cycling

the symmetric K/K-beta"-alumina/K cell at successively higher current densities until cell failure (Fig. 2) [27]. This was carried out at a temperature of 20 °C with the cell under a constant stack-pressure of 2.5 MPa. Cycling was initiated at a current density of 0.05 mA/cm^2, then raised to 0.1 mA/cm^2 for the second cycle, and thereafter increased in steps of 0.1 mA/cm^2 until cell failure was observed at 4.8 mA/cm^2. The critical current for dendrite growth of 4.8 mA/cm^2 is amongst the highest values reported in the literature for a solid metal anode/SE interface and demonstrates that the K/K-beta"-alumina interface is able to sustain high rates of charge [28–31]. It should be noted that polarisation is observed for current densities greater than approximately 2 mA/cm^2, suggesting that some voiding is occurring when stripping at these high current rates, leading to a reduced metal anode/SE contact area. As such, 4.8 mA/cm^2 may even be an underestimate of the true areal critical current for dendrite penetration.

Further to the problem of electrode/SE contact loss at high currents, the critical current for void formation during stripping was determined by cycling 3-electrode cells, with the critical current determined to have been exceeded when cell polarisation was observed during stripping (Fig. 3) [13, 16, 17]. At a current density of 1 mA/cm^2 (Fig. 3a), no increase in cell polarisation was observed over 25 cycles. When cycling at 2 mA/cm^2 (Fig. 3b), only a very slight cell polarisation was observed, increasing from 43 mV at the end of the first stripping (red) to 54 mV at the end of the 25th stripping (green). By contrast, significant polarisation on stripping was observed when cycling at 3 mA/cm^2 (Fig. 3c), increasing from 70 to 120 mV through the course of the first cycle (red), worsening with cycle number to reach 149 mV at the end of the 25th cycle (green). It can therefore be concluded that under a stack-pressure of 2.5 MPa and at 20 °C, the critical current for voiding on stripping is at approximately 2 mA/cm^2 and has been exceeded at 3 mA/cm^2.

These results are in agreement with SEMs showing the cross-sections of the stripped K/K-beta"-alumina interface after 25 cycles. After cycling at 1 mA/cm^2, below the critical current for void formation, the interface between K and K-beta"-alumina remains highly conformal, with no contact loss observed (Fig. 4a). By contrast, numerous voids are observed in the K metal anode after cycling at 3 mA/cm^2, above the critical current for voiding (Fig. 4b). What is more, severe dendrite penetration into the K-beta"-alumina at areas around the interfacial voids is observed, confirmed by the K EDS signal (turquoise) within the electrolyte (Fig. 4bii). The presence of dendrites on cycling at 3 mA/cm^2 is not surprising, despite the critical current for dendrite penetration, reported above, being higher at 4.8 mA/cm^2, as voiding reduces the area of contact between the K electrode and K-beta"-alumina electrolyte, leading to higher local current densities. These local current densities can exceed the high critical current density for dendrite growth of 4.8 mA/cm^2, despite the nominal areal current density being only 3 mA/cm^2 [13]. Further magnified micrographs of the K dendrite morphology within the K-beta"-alumina are shown in Supplementary Fig. 2.

The critical current for void formation in the K metal anode of ~ 2 mA/cm^2 under a 2.5 MPa stack-pressure and 20 °C is higher than typically observed for Li anodes; for example 0.2 mA/cm^2 under 3 MPa pressure for the Li/Li_6PS_5Cl interface [13], and 0.2 mA/cm^2 under 3.2 MPa pressure for the Li/$Li_7La_3Zr_2O_{12}$ interface [32]. Together with the relatively high critical current for plating, the results show K metal anodes are not only less rate limited during the K metal plating process during charge but also during the K metal stripping process on discharge.

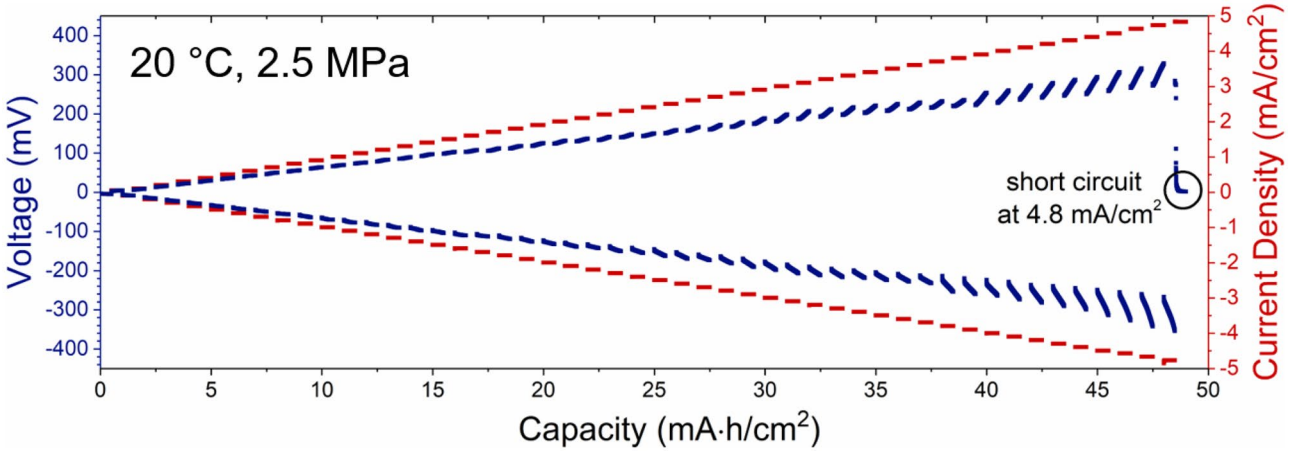

Fig. 2 Cycling of a K/K-beta"-alumina/K symmetric cell, showing the voltage response (blue) when the current density (red) is increased in steps each cycle until cell failure at a current density of 4.8 mA/cm^2. Cycling was carried out at 20 °C under a 2.5 MPa stack-pressure, moving 0.5 mA·h/cm^2 capacity each half cycle

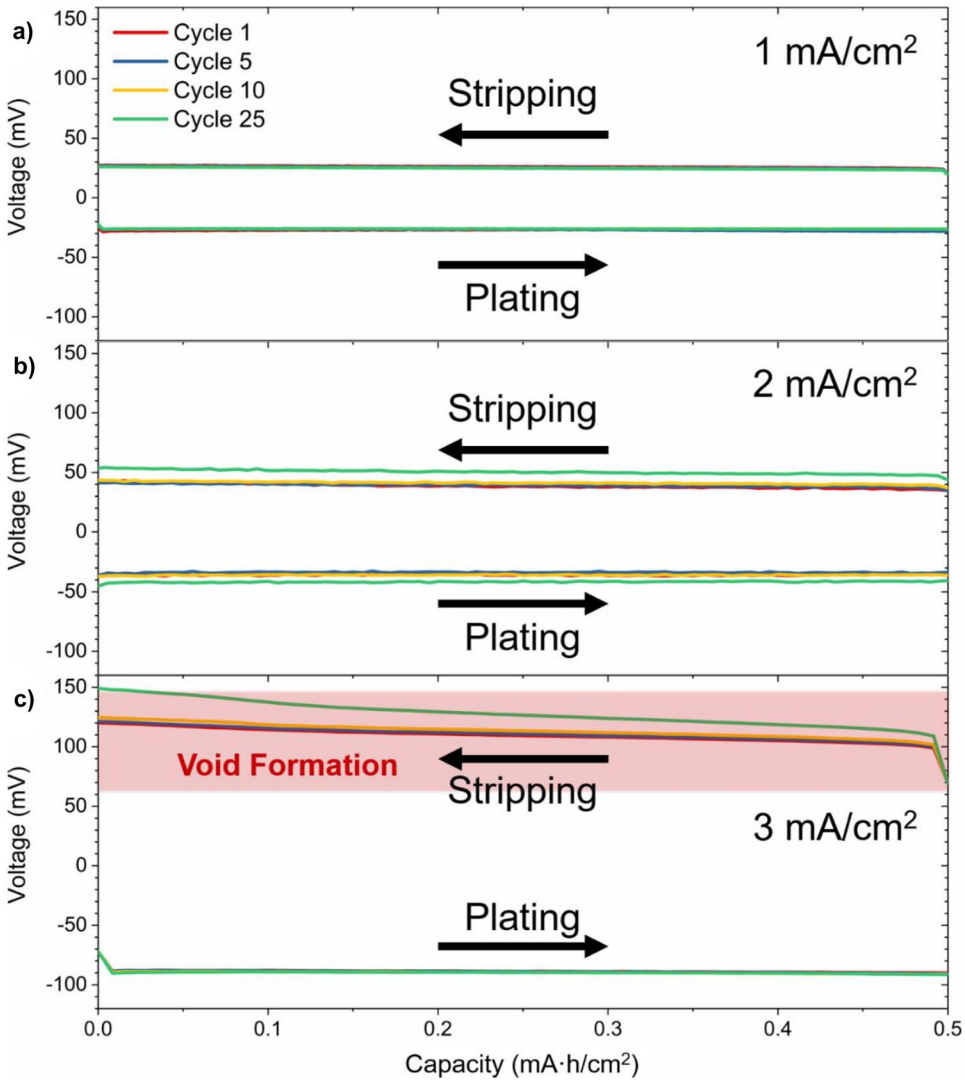

Fig. 3 3-Electrode K/K-beta"-alumina cells with a K metal reference electrode showing 25 cycles at current densities of **a** 1 mA/cm^2, **b** 2 mA/cm^2, and **c** 3 mA/cm^2. Cycling was carried out at 20 °C under a 2.5 MPa stack-pressure, moving 0.5 mA·h/cm^2 capacity each half cycle, beginning by plating the working electrode (and stripping the counter electrode). Cell polarisation when stripping at 3 mA/cm^2 indicates voiding at the K/K-beta"-alumina interface

Considering the models that have been proposed to explain dendrite penetration through ceramic electrolytes, they generally involve the alkali metal filling cracks or pores in the electrolyte near the anode/electrolyte interface [33–36]. Fracture of the SE can occur when the rate of metal plating into a near-surface crack or pore exceeds the rate of extrusion from the crack or pore into the bulk of the metal anode. Softer metals that are more ductile and flow more easily can extrude from the ceramic more readily, meaning that failure requires higher plating currents such that the rate of plating exceeds extrusion. Passing down the alkali metal column in the periodic table, the yield strengths decrease from approximately 1.74 MPa for Li, to 0.41 MPa for Na and 0.24 MPa for K [14, 37–40]. As such, K metal will yield and be extruded more readily from surface cracks and flaws than Li or Na, and therefore, critical currents for dendrite penetration would be expected to be higher, all else being equal.

Similarly, the critical current for voiding also depends on the mechanical properties of the metal anode [16, 17, 41, 42]. Voiding occurs when the flux of ions away from the interface under current load exceeds the transport of metal atoms to the interface [13, 43, 44]. The mechanisms by which metal atoms are transported to the interface are by self-diffusion and, when the cell is under a stack-pressure, creep [13, 45, 46]. Lower yield strength materials such as K creep more readily, and the activation energy of mono-vacancy self-diffusion is lower for K than Li or Na [47]. Therefore, K metal will sustain higher stripping currents than Li or Na metal anodes before voids form at the interface [16]. The high critical currents for both dendrite penetration and voiding observed in this work help to verify these models for failure on plating and stripping, confirming that both failures are strongly dependant on the mechanical properties of the metal anode, with low yield strength metal anodes giving higher critical currents. However, whilst the critical currents for dendrite penetration and voiding are dependent on the properties of the metal anode, they also have dependence on other factors; for example, voiding also

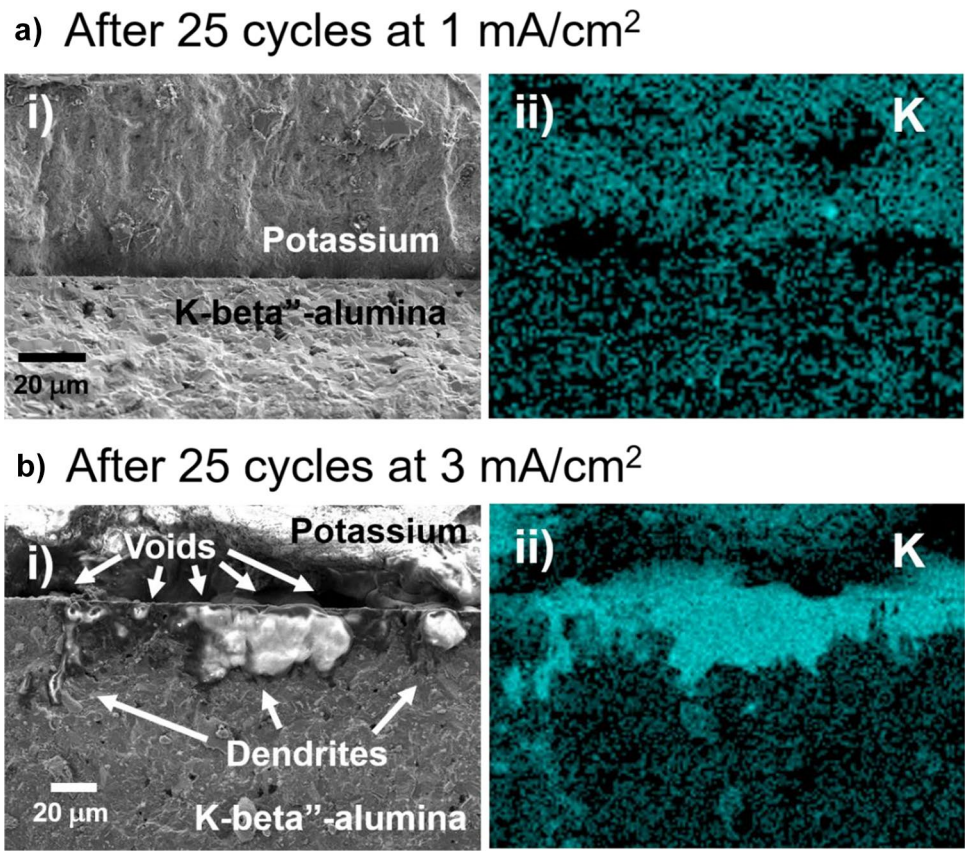

Fig. 4 **a** K/K-beta"-alumina interface after the 25th stripping when cycling at 1 mA/cm^2 and **b** K/K-beta"-alumina interface after the 25th stripping when cycling at 3 mA/cm^2. (i) Scanning electron micrographs and (ii) Energy Dispersive X-ray Spectrometry colour map showing K signal (turquoise)

depends on the adhesion of the metal anode to the solid electrolyte [42], and dendrite growth depends not only on the properties of the metal anode but also on the properties of the SE [33–35].

Conclusions

An exploration of dendrite penetration and voiding in solid-state cells with a potassium anode and potassium ion conducting solid electrolyte, K-beta"-alumina, reveals relatively high critical currents compared with Li and Na metal anode SSBs. Failure of a K/K-beta"-alumina/K symmetric cell due to dendrites, which penetrate the SE when plating K metal, was observed at a current density of 4.8 mA/cm^2. Similarly, the formation of voids in the K anode at the K/K-beta"-alumina interface was determined to occur at a stripping current of 2 mA/cm^2. It is concluded that K anode SSBs are able to sustain relatively high rates of K metal plating and stripping without failure due to the mechanical properties of K metal, with its low yield strength and readiness to creep under relatively low stack-pressures enabling high rates of charge and discharge.

Supplementary Information The online version contains supplementary material available at https://doi.org/10.1007/s10008-022-05225-8.

Acknowledgements P.G.B. is indebted to the Faraday Institution All-Solid-State Batteries with Li and Na Anodes (FIRG007, FIRG008), the Engineering and Physical Sciences Research Council (EP/M009521/1) and The Henry Royce Institute for Advanced Materials for financial support (EP/R00661X/1, EP/S019367/1, EP/R010145/1).

References

1. Janek J, Zeier WG (2016) A solid future for battery development. Nat Energy 1:16141

2. Pasta M et al (2020) Roadmap on solid-state batteries. J Phys Energy 2:0–52
3. Kerman K, Luntz A, Viswanathan V, Chiang Y-M, Chen Z (2017) Review - Practical challenges hindering the development of solid state li ion batteries. J Electrochem Soc 164:A1731–A1744
4. Yu Z et al (2021) Dendrites in solid-state batteries: ion transport behavior, advanced characterization, and interface regulation. Adv Energy Mater 11:1–25
5. Cao D et al (2020) Lithium dendrite in all-solid-state batteries: growth mechanisms, suppression strategies, and characterizations. Matter 3:57–94
6. Lou S et al (2021) Interface issues and challenges in all-solid-state batteries: lithium, sodium, and beyond. Adv Mater 33:1–29
7. Jow TR, Liang CC (1983) Interface between solid electrode and solid electrolyte - a study of the Li/LiI(AI_2O_3) solid-electrolyte system. J Electrochem Soc 130:737–740
8. Koshikawa H et al (2018) Dynamic changes in charge-transfer resistance at Li metal/$Li_7La_3Zr_2O_{12}$ interfaces during electrochemical Li dissolution/deposition cycles. J Power Sources 376:147–151
9. Meyer M, Rickert H, Schwaitzer U (1983) Investigations on the kinetics of the anodic dissolution of lithium at the interface Li/Li_3N. Solid State Ionics 9–10:689–693
10. Hatzell KB et al (2020) Challenges in lithium metal anodes for solid-state batteries. ACS Energy Lett 5:922–934
11. Rees GJ et al (2020) Imaging sodium dendrite growth in all-solid-state sodium batteries using ^{23}Na T2-weighted MRI. Angew Chemie Int Ed 133:2138–2143
12. Lewis J et al (2020). Linking void and interphase evolution to electrochemistry in solid-state batteries using operando X-ray tomography. https://doi.org/10.26434/chemrxiv.12468170
13. Kasemchainan J et al (2019) Critical stripping current leads to dendrite formation on plating in lithium anode solid electrolyte cells. Nat Mater 18:1105–1111
14. Park RJY et al (2021) Semi-solid alkali metal electrodes enabling high critical current densities in solid electrolyte batteries. Nat Energy 6:314–322
15. Bryan K et al (2021) Operando analysis of the molten Li|LLZO interface: understanding how the physical properties of Li affect the critical current density. Matter 4:1947–1961
16. Spencer Jolly D et al (2020) Sodium/Na β″ alumina interface: effect of pressure on voids. ACS Appl Mater Interfaces 12:678–685
17. Spencer Jolly D et al (2021) Temperature dependence of lithium anode voiding in argyrodite solid-state batteries. ACS Appl Mater Interfaces 13:22708–22716
18. Bay M et al (2020) Sodium plating from Na-β″-alumina ceramics at room temperature, paving the way for fast-charging all-solid-state Batteries. Adv Energy Mater 10:1902899
19. Baffier N, Badot JC, Colomban P (1981) Conductivity of ion rich β and β" alumina: sodium and potassium compounds. Mater Res Bull 16:259–265
20. Baclig AC et al (2018) High-voltage, room-temperature liquid metal flow battery enabled by na-K|K-β″-alumina stability. Joule 2:1287–1296
21. Sharafi A et al (2017) Surface chemistry mechanism of ultra-low interfacial resistance in the solid-state electrolyte $Li_7La_3Zr_2O_{12}$. Chem Mater 29:7961–7968
22. Spencer Jolly D et al (2022) Interfaces between ceramic and polymer electrolytes: a comparison of oxide and sulfide solid electrolytes for hybrid solid-state batteries. Inorganics 10:1–13
23. Sharafi A, Meyer HM, Nanda J, Wolfenstine J, Sakamoto J (2016) Characterizing the Li-$Li_7La_3Zr_2O_{12}$ interface stability and kinetics as a function of temperature and current density. J Power Sources 302:135–139
24. Irvine JTS, Sinclair DC, West AR (1990) Electroceramics characterized by impedance spectroscopy. Adv Mater 2:132–138
25. Shchukarev AV, Korolkov DV (2004) XPS study of group IA carbonates. Cent Eur J Chem 2:347–362
26. Greczynski G, Hultman L (2017) C 1s peak of adventitious carbon aligns to the vacuum level: dire consequences for material's bonding assignment by photoelectron spectroscopy. ChemPhysChem 18:1507–1512
27. Lu Y et al (2021) Critical current density in solid-state lithium metal batteries: mechanism, influences, and strategies. Adv Funct Mater 2009925:1–33
28. Pervez SA, Cambaz MA, Thangadurai V, Fichtner M (2019) Interface in solid-state lithium battery: challenges, progress, and outlook. ACS Appl Mater Interfaces. https://doi.org/10.1021/acsami.9b02675
29. Wang MJ, Kazyak E, Dasgupta NP, Sakamoto J (2021) Transitioning solid-state batteries from lab to market: linking electro-chemo-mechanics with practical considerations. Joule 5:1371–1390
30. Lewis JA, Tippens J, Cortes FJQ, McDowell MT (2019) Chemo-mechanical challenges in solid-state batteries. Trends Chem 1:845–857
31. Albertus P et al (2021) Challenges for and pathways toward Li-metal-based all-solid-state batteries. ACS Energy Lett 6:1399–1404
32. Wang MJ, Choudhury R, Sakamoto J (2019) Characterizing the Li-solid-electrolyte interface dynamics as a function of stack pressure and current density. Joule 1–14. https://doi.org/10.1016/j.joule.2019.06.017
33. Porz L et al (2017) Mechanism of lithium metal penetration through inorganic solid electrolytes. Adv Energy Mater 7:1–12
34. Barroso-Luque L, Tu Q, Ceder G (2020) An analysis of solid-state electrodeposition-induced metal plastic flow and predictions of stress states in solid ionic conductor defects. J Electrochem Soc 167:020534
35. Feldman LA, De Jonghe LC (1982) Initiation of mode I degradation in sodium-beta alumina electrolytes. J Mater Sci 17:517–524
36. Ning Z et al (2021) Visualizing plating-induced cracking in lithium-anode solid-electrolyte cells. Nat Mater 20:1121–1130
37. Masias A, Felten N, Garcia-mendez R, Wolfenstine J, Sakamoto J (2019) Elastic, plastic, and creep mechanical properties of lithium metal. J Mater Sci 54:2585–2600
38. Wang MJ, Chang JY, Wolfenstine JB, Sakamoto J (2020) Analysis of elastic, plastic, and creep properties of sodium metal and implications for solid-state batteries. Materialia 12:28
39. Fincher CD, Ojeda D, Zhang Y, Pharr GM, Pharr M (2020) Mechanical properties of metallic lithium: from nano to bulk scales. Acta Mater 186:215–222
40. Fincher CD, Zhang Y, Pharr GM, Pharr M (2020) Elastic and plastic characteristics of sodium metal. ACS Appl Energy Mater. https://doi.org/10.1021/acsaem.9b02225
41. Zhang X, Wang QJ, Harrison KL, Roberts SA, Harris SJ (2020) Pressure-driven interface evolution in solid-state lithium metal batteries. Cell Reports Phys Sci 1:100012
42. Seymour ID, Aguadero A (2021) Suppressing void formation in all-solid-state batteries: the role of interfacial adhesion on alkali metal vacancy transport. J Mater Chem A. https://doi.org/10.1039/d1ta03254b
43. Shishvan SS, Fleck NA, Deshpande VS (2021) The initiation of void growth during stripping of Li electrodes in solid electrolyte cells. J Power Sources 488:229437
44. Yang M, Liu Y, Nolan AM, Mo Y (2021) Interfacial atomistic mechanisms of lithium metal stripping and plating in solid-state batteries. Adv Mater 33:1–12
45. Krauskopf T, Hartmann H, Zeier WG, Janek J (2019) Toward a fundamental understanding of the lithium metal anode in solid-state batteries - an electrochemo-mechanical study on the garnet-type solid electrolyte $Li_{6.25}Al_{0.25}La_3Zr_2O_{12}$. Appl Interfaces Mater 14463–14477. https://doi.org/10.1021/acsami.9b02537

46. Krauskopf T, Richter FH, Zeier WG, Janek J (2020) Physicochemical concepts of the lithium metal anode in solid-state batteries. Chem Rev. https://doi.org/10.1021/acs.chemrev.0c00431
47. Schott V, Fähnle M, Madden PA (2000) Theory of self-diffusion in alkali metals: I. Results for monovacancies in Li, Na, and K. J Phys Condens Matter 12:1171–1194